Acquisition of the Wide Swath Significant Wave Height From HY-2C Through Deep Learning

Jichao Wang[1,1], Ting Yu[1,1], Fangyu Deng[1,1], Yongjun Jia[2,2], and Zongli Ruan[1]

[1]China University of Petroleum
[2]National Satellite Ocean Application Service

November 30, 2022

Abstract

The significant wave height (SWH) is of great importance in industries such as ocean engineering, marine resource development, shipping and transportation. Haiyang-2C (HY-2C), the 2nd operational satellite of China's marine dynamic exploration series, can provide all-weather, all-day, global observations of wave height, wind, and temperature. In this paper, a deep learning approach is applied to build a wide swath model based on the SWH from the altimeter and the wind speed from the scatterometer of HY-2C. Two validation sets, 1-month data at 6-minute intervals and 1-day data with an interval of 10 s, are fed into the trained model. Experiments indicate that the extending nadir SWH yields a real-time wide swath grid product along track, which can be offered as support for oceanographic study, and it is superior to take the swell characteristics of ERA5 into account as the input of wide swath SWH model. In conclusion, the verification results demonstrate the effectiveness and feasibility of the wide swath SWH model.

Hosted file

essoar.10508123.2.docx available at https://authorea.com/users/560522/articles/608502-acquisition-of-the-wide-swath-significant-wave-height-from-hy-2c-through-deep-learning

Article

Acquisition of the Wide Swath Significant Wave Height From HY-2C Through Deep Learning

Jichao Wang [1], **Ting Yu** [1], **Fangyu Deng** [1], **Zongli Ruan** [1] and **Yongjun Jia** [2],*

1   College of science, China University of Petroleum, Qingdao 266580, Shandong, China.
2   National Satellite Ocean Application Service, Beijing 100081, China.
*   Correspondence: jiayongjun@mail.nsoas.org.cn.

Abstract: The significant wave height (SWH) is of great importance in industries such as ocean engineering, marine resource development, shipping and transportation. Haiyang-2C (HY-2C), the 2nd operational satellite of China's marine dynamic exploration series, can provide all-weather, all-day, global observations of wave height, wind, and temperature. The altimeter can only measure the nadir wave height and other information, and the scatterometer can obtain the wind field with a wide swath. In this paper, a deep learning approach is applied to produce a wide swath SWH data through the wind field from the scatterometer and the nadir wave height from altimeter. Two validation sets, 1-month data at 6-minute intervals and 1-day data with an interval of 10 s, are fed into the trained model. Experiments indicate that the extending nadir SWH yields a real-time wide swath grid product along track, which can be offered as support for oceanographic study, and it is superior to take the swell characteristics of ERA5 into account as the input of wide swath SWH model. In conclusion, the verification results demonstrate the effectiveness and feasibility of the wide swath SWH model.

Keywords: HY-2C; Deep Learning; the Wide Swath Significant Wave Height

1. Introduction

Significant wave height (SWH) is the most widely utilized wave parameter in climate assessment and various marine industries. Providing in situ observations, wave buoys are traditional measurement tools of SWH that can provide diverse and comprehensive information and are studied extensively in researches [1−3]. However, the single-point measurement has sparse, irregular, and limited spatial coverage, thus wider spatial coverage is of general interest. Satellite altimeters can quickly and accurately measure the global sea surface height, and their measurement accuracy has reached the centimeter level. The acquired SWH from Geosat [4], Jason-1 and Envisat [5], SARAL/AltiKa [6 − 8], Sentinel 3A and 3B [9 − 10], Haiyang-2 series [11 − 14], Chinese-French Oceanography Satellite (CFOSAT) [15–16] altimeter (ALT) are validated by comparison with those of the buoys from the National Data Buoy Center. For the ALT data, the measurements remain restricted to the nadir tracks, which greatly limits the number of observations.

Haiyang-2C (HY-2C), China's third marine dynamic environment satellite, is subordinate to the HY-2 marine remote sensing satellite series. HY-2C combines visible/infrared and microwave sensors, with high-precision orbit measurement, orbit determination capabilities, and all-weather, all-day, and global detection capabilities. Thus, it provides support services for marine resources development, marine environmental protection, and national defense construction, etc.

Deep learning is a class of efficient algorithms for learning representative and discriminative input features in a hierarchical manner [17], which has become a hot

topic in various fields, particularly in marine remote sensing, such as classifying oceanographic objects from Synthetic Aperture Radar (SAR) data [18], retrieving sea surface wind speed in SAR images [19–20], providing higher accuracy wave parameters [21–23], etc. It is worth noting that Wang et al. [24] developed a deep learning approach for retrieving the SWH over an extended swath via a CFOSAT with simultaneous wind and wave observations. As a matter of fact, we attempt to find a more specific deep neural network using fewer input features to retrieve a wider swath of SWH. The gate recurrent unit (GRU) network is designed to solve the gradient disappearance problem that occurs in standard recurrent neural network, and is a popular and creditable choice because of its simple structure, fast training speed, and dominant effect.

In this paper, we adopt a deep learning method to obtain a wide swath SWH from simultaneous observations of radar ALT and microwave scatterometer (SCA) of HY-2C. First, the nadir SWH obtained by ALT is employed to select the wind speed of SCA, where the time difference is less than 5 s, and we spatially choose the closest wind column. Approximately eight months (from Sep. 25, 2020 to Jun. 1, 2021) of the HY-2C and ERA5 collected datasets are considered and matched. In the configuration cases, the matching criteria are set within 100 km for geographical distance and half an hour for temporal difference. Then the validation set is divided by a length of 300, and the statistical results are analyzed through the leftmost, center and rightmost columns located in the wide swath SWH, in order to illustrate the performance of the wide swath SWH model in each segmented interval. Finally, the results of the 1-day validation set at 10-second intervals are discussed, and two small areas are selected and drawn separately to demonstrate the validation effect of the wide swath SWH model at different ranges of numerical variation.

The structure of this paper can be summarized as follows: Section 2 introduces the characteristics of HY-2C and ERA5, as well as adopted method and datasets. Section 3 compares and analyzes the performance of the model. Finally, Section 4 concludes this paper.

2. Data and Method

Haiyang-2C (HY-2C) was successfully launched on September 21, 2020 at the Jiuquan Satellite Launch Center in Inner Mongolia, China. Unlike the HY-2B satellite in a polar orbit, the HY-2C satellite operates in an inclined orbit [25], which travels at an altitude of 1336 km and presents an orbital inclination angle of 66°. Thus, it achieves the purpose of accelerating satellite revisit to the area within 70 degrees north south from the equator, shortening the observations interval of the region, and improving the observations efficiency. HY-2C, the first large-scale inclined orbit remote sensing satellite, was constructed under the National Civil Space Infrastructure Plan [26]. The satellite adopts an orbit with regression periods of 10 and 400 days in the early and later stage, respectively.

The main function of the ALT is to measure the global sea surface height, SWH and gravity field parameters and the ALT has an external calibration working mode that can cover the complete calibration area. Its operating frequency denotes13.58 GHz, 5.25 GHz, pulse limited footprint is better than 2 km, and the range accuracy of marine nadir point is better than 2 cm. Although the HY-2C ALT provides SWH in Ku and C bands, we select only Ku-band measurements as experimental data in this paper due to its higher accuracy, and the fact that the C-band is designed mainly to modify the path delay caused by ionosphere during Ku-band ALT [27].

HY-2C carries a Ku-band rotating pencil-beam SCA in a non-sun-synchronous orbit. As the main payload of marine dynamic environment, SCA has a coverage rate of not less than 90% in the global sea area for 1 to 2 days. Its main function is to measure the wind vector field (Figure 1), and the accuracy of wind direction and wind speed measurement are better than 15° and 1.5 m/s, respectively. It also has an external calibration working mode with an operating frequency of 13.256 GHz and two beams,

which are HH polarization for the internal beam and VV polarization for the external beam. Moreover, Wang et al. [28] verified the wind product of the SCA and believed its great availability.
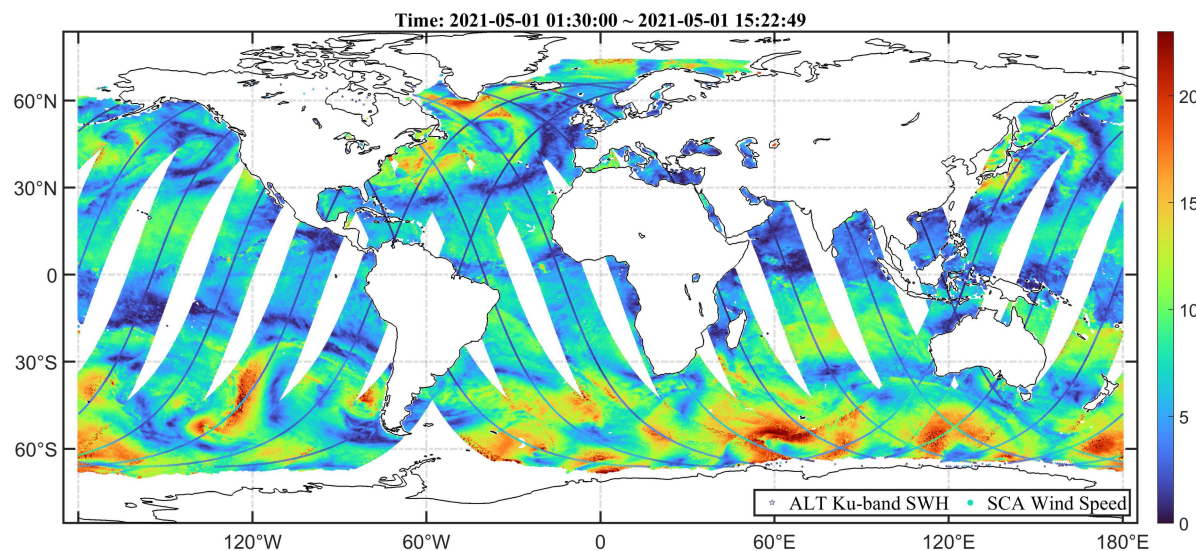
Figure 1. Information of the wind speed from SCA and the Ku-band SWH from ALT are obtained simultaneously from HY-2C on May 1, 2021.

ERA5 is a global climate reanalysis datasets released by the European Center for Medium-Range Weather Forecasts. It has the advantages of high spatial resolution, hourly atmospheric, terrestrial and ocean climate variables, 3-hourly uncertainty information, more satellite observations, and accessing to all input observations [29]. The collected SWH has a resolution of 0.25° longitude by 0.25° latitude in space and hourly in time.

The wind and wave from remote sensing data and the wave from analysis datasets have different types of property, and they are regarded as necessary features and labels for purpose of verifying the effectiveness of the data. Therefore, the SWH of ERA5 are compared with the observations of HY-2C ALT, the wind speed of ERA5 are by contrast with SCA L2B product, as shown in Figure 2.
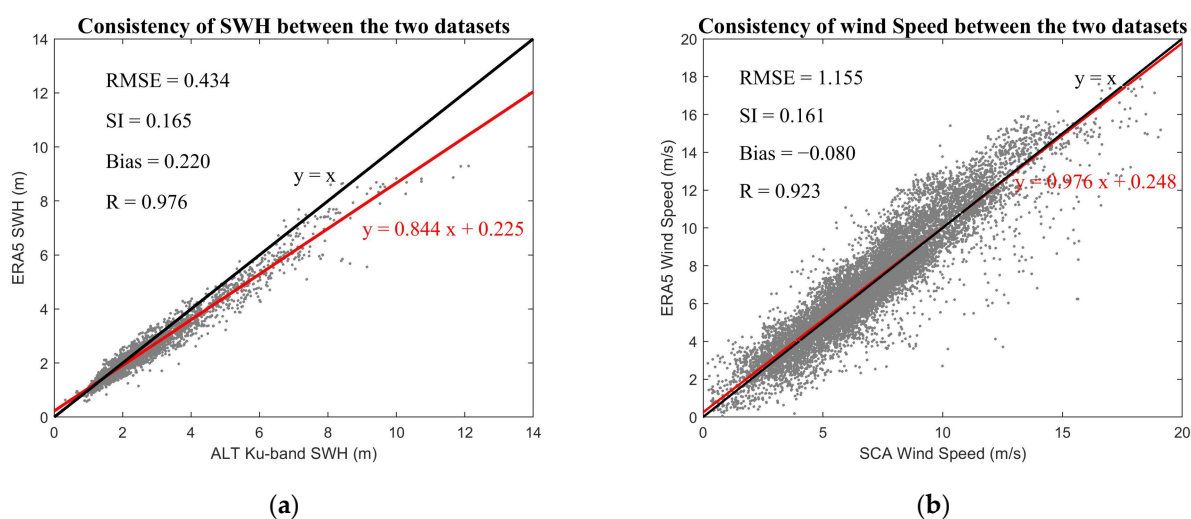
Figure 2. Scatter plots of SWH (**a**) and wind speed (**b**) from HY-2C and ERA5 to check the consistency. The red lines indicate the linear fit and the black lines mean the full correlation.

118 It can be seen that both SWH and wind speed show great consistency, indirectly
119 indicating that it is reasonable to use matched ERA5 SWH as labels at the space and time
120 scales, further proving the feasibility of the model. The statistical metrics, namely, root
121 mean square error (RMSE), scattering index (SI), bias (Bias), and the Pearson correlation
122 coefficient (R), are applied to measure the effectiveness of the data and model, defined
123 as follows.

$$RMSE = \sqrt{\frac{1}{N}\sum_{t=1}^{N}(y_o^t - y_v^t)^2}$$

$$SI = RMSE/mean(y_o)$$

$$Bias = \sum_{t=1}^{N}(y_o^t - y_v^t)$$

$$R = \frac{\sum_{t=1}^{N}(y_o^t - mean(y_o))(y_v^t - mean(y_v))}{\sqrt{\sum_{t=1}^{N}(y_o^t - mean(y_o))^2}\sqrt{\sum_{t=1}^{N}(y_v^t - mean(y_v))^2}}$$

124 where y_v^t and y_o^t are validation and observations, respectively.
125 Deep learning approaches can be capable of handling various problems and have
126 been widely applied in various directions. Its attached GRU model possesses two unique
127 gating devices, the reset gate r_t and the update gate z_t, to make a selection between the
128 input x_t and the state of hidden layer unit at the previous moment h_{t-1}, enabling the
129 model to preserve important features in the long-term sequence. Intuitively speaking,
130 the reset gate r_t determines the chosen characteristics of combining x_t with h_{t-1}, and
131 the update gate z_t defines the information saved from the candidate state $\tilde{h}_t$ to the
132 current moment hidden state h_t (Figure 3a). The GRU model consists of five layers of
133 neurons. The weights and biases between the neurons are iterated and updated during
134 the training process, using the adaptive moment estimation optimizer and the mean
135 square error loss function as supervision to create a wide swath model. The main
136 parameters of the model are the batch size, the number of hidden layers, the number of
137 hidden units per layer, the learning rate and iterations, which take the values of 20, 3, 20,
138 0.001, and 500, respectively.

139

(**a**) (**b**)
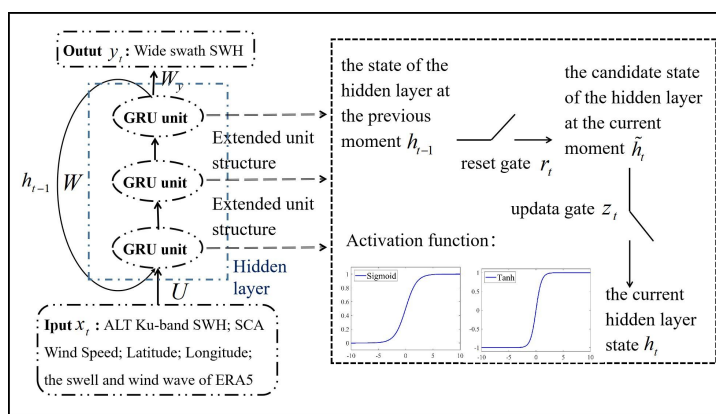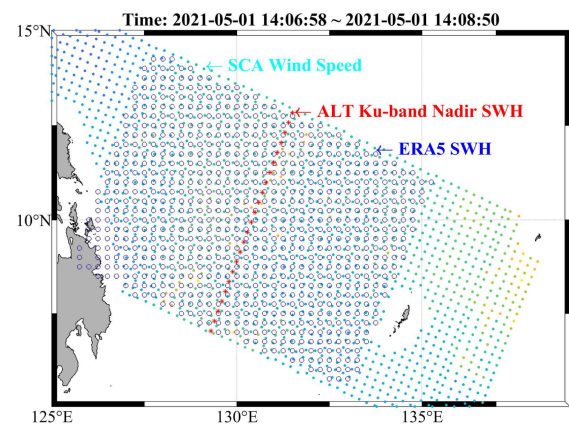
140 **Figure 3.** (**a**) The structure diagram of the GRU network to obtain the wide swath SWH; (**b**) A schematic diagram of the
141 data parameters and widths acquired by the ALT, SCA, and ERA5. It is worth noting that the widths displayed by ERA5
142 are selected according to comprehensive consideration of model efficiency and effectiveness.

143 To make width of the nadir SWH close to the dimension of SCA wind speed,
144 different parameters are considered as inputs, including the nadir SWH, latitude, and

longitude acquired by ALT, the wind speed collected by SCA L2B product, as well as swell, wind wave, and SWH obtained by ERA5. We first give the nadir SWH at six-minute intervals and apply their geographical location and corresponding moment for the selection of the derived wind speed. Wind speed and SWH are acquired on different instruments at the same time, but the presence of missing data requires the latter to be employed as a reference to filter the former using the time difference no more than 5 s (Figure 3b). In addition, the distance between the SCA grid and matched data by ERA5 is limited to less than 100 km, the time window denotes ± 30 min, and the width of the matched SWH account for half of the wind field in accordance with the efficiency and benefit. The latitude range is selected between $60\,^{\circ}$ S and $60\,^{\circ}$ N due to the validity and large probability distribution of the data. The scope of the training data set is from September 25, 2020 to April 25, 2021 for seven months, while the validation data set represents independent one-month with the time range from May 1, 2021 to June 1, 2021.

3. Results and analysis

Wide-dimensional fields have more information and data volume. We utilize the wind speed and SWH simultaneously retrieved by HY-2C as features and the SWH obtained by ERA5 as labels, so that a wide swath model can be built. It is well known that the ALT data are generated almost per second. Based on the dual consideration of runtime and the amount of data, we extract the nadir SWH at six-minute intervals and filter the data with a length of 15,360 samples in the training set. While for the validation set, we execute the same operation with an integration length of 2500 observations. The swell and wind wave information in ERA5 has a certain effect on the building of wide swath SWH model, for which we gather the relevant data after matching based on the latitude and longitude of the nadir SWH, and apply them as the input features of Experiments 2 and 3, respectively. The other parameters and settings remain unchanged. The processed datasets are fed into the GRU model, thereby the validation set results are shown in Table 1.

Table 1. Numerical results of the validation set in the GRU model with different input features.

Input features of experiments 1-3	RMSE	SI	Bias	R
Experiment 1: Wind and SWH simultaneously acquired by HY-2C, Latitude, and Longitude	0.4056	0.1528	0.0154	0.9428
Experiment 2: Wind and SWH simultaneously acquired by HY-2C, Latitude; Longitude, and Swell obtained from ERA5	0.3696	0.1381	$-$0.0069	0.9530
Experiment 3: Wind and SWH simultaneously acquired by HY-2C, Latitude, Longitude, and Wind wave collected from ERA5	0.4344	0.1629	0.0032	0.9353

Table 1 depicts that the swell presents a positive influence on the establishment of wide swath SWH model, on the contrary, the wind wave has a negative impact on it. For example, compared to RMSE of the Experiment 1, that of the Experiment 2 decreases 0.0360 m, which indicates that the model performance is improved, while that of the Experiment 3 increases 0.0288 m, implying more inefficient the model output. Wind wave mainly exhibits sharp peak, which is prone to wave breaking when the wind remains strong, while swell presents smoother, with long and regular wave lines. The wide swath SWH model concentrates on long-term features in the process of learning wind and wave characteristics, while for wind wave, it behaves as local features. Overall, we mainly focus on the first two experiments in the following analysis.

Three columns of data with a length of 300 on the leftmost, center, and rightmost sides of wide swath SWH are selected as representatives to further analyze the performance of different stages. In Table 2, the three columns numerical results of Experiment 1 are shown that the center column has better results than the other two columns under arbitrary segmented data. The reason for this phenomenon may be that the larger the distance between both sides of the nadir SWH and the center, the less the importance of the wind in the modeling process, and the worse the effect on the nadir SWH.

In the segmented data, the validation results of the three columns for Interval 1 are the worst among those for all intervals. For Interval 5, its leftmost and rightmost columns show superior values, its center column is excellent and second only to the center column for Interval 4. We count the total number of points with SWH less than 1 m (troughs) and greater than 7 m (peaks) for each phase. Results indicate that Interval 1 has 332 minimal and maximal points, and these local features gradually disappear during the process of training, resulting in inferior performance. Surprisingly, Interval 5 has only 85 extreme points, thus dominates the results. Based on the above analysis, Interval 5 (bolder words in Table 2), which locates in the middle of validation set and remains superior, is selected to display the range and validation results of the three columns of data, as shown in Figure 4.

Table 2. The numerical results of the segmented data on the leftmost, center, and rightmost columns in Experiment 1.

| Segmented data in the validation set		RMSE	SI	Bias	R
Interval 1: 1-300	The leftmost column	0.6785	0.2633	0.0210	0.8449
	The center column	0.6023	0.2319	–0.0079	0.8931
	The rightmost column	0.7392	0.2813	–0.0524	0.8280
Interval 2: 301-600	The leftmost column	0.4650	0.1740	–0.0277	0.9280
	The center column	0.2577	0.0966	0.0351	0.9797
	The rightmost column	0.5155	0.1928	–0.0018	0.9041
Interval 3: 601-900	The leftmost column	0.4632	0.1725	–0.0038	0.9335
	The center column	0.2862	0.1064	0.0323	0.9779
	The rightmost column	0.4687	0.1716	–0.0160	0.9333
Interval 4: 901-1200	The leftmost column	0.4623	0.1734	0.0580	0.9293
	The center column	0.2420	0.0891	–0.0137	0.9820
	The rightmost column	0.4484	0.1623	–0.0239	0.9453
Interval 5: 1201-1500	**The leftmost column**	**0.4289**	**0.1680**	**0.0244**	**0.9180**
	The center column	**0.2554**	**0.0996**	**0.0221**	**0.9731**
	The rightmost column	**0.4155**	**0.1591**	**0.0197**	**0.9279**
Interval 6: 1501-1800	The leftmost column	0.4712	0.1776	0.0426	0.9037
	The center column	0.2844	0.1072	0.0308	0.9688
	The rightmost column	0.4954	0.1843	–0.0100	0.9100
Interval 7: 1800-2100	The leftmost column	0.4438	0.1711	0.0528	0.9128
	The center column	0.2673	0.1034	0.0175	0.9662
	The rightmost column	0.5030	0.1906	–0.0454	0.8819
Interval 8: 2101-2400	The leftmost column	0.5086	0.1875	0.0737	0.9323
	The center column	0.2798	0.1026	0.0610	0.9763
	The rightmost column	0.4834	0.1758	0.0446	0.9268

Comparing Figure 4a-c, it can be found that the center column can evaluate the peaks, while SWH on the leftmost and rightmost columns are generally underestimated at the peaks and slightly overestimated at the troughs, which are consistent with the experimental results obtained in Table 2. Although the red line is not as good as the blue line in Figure 4b for some peaks, it has a better fit between 1 and 5 m. To summarize, the

results of the segmented interval in the three columns of data has an acceptable performance, understanding the effectiveness of the model. To distinctly demonstrate the accuracy of the model, the validation results for 1 day (from May 1 to May 2, 2021) with 10-second intervals are plotted in Figure 5.

(**a**)

(**b**)

(**c**)
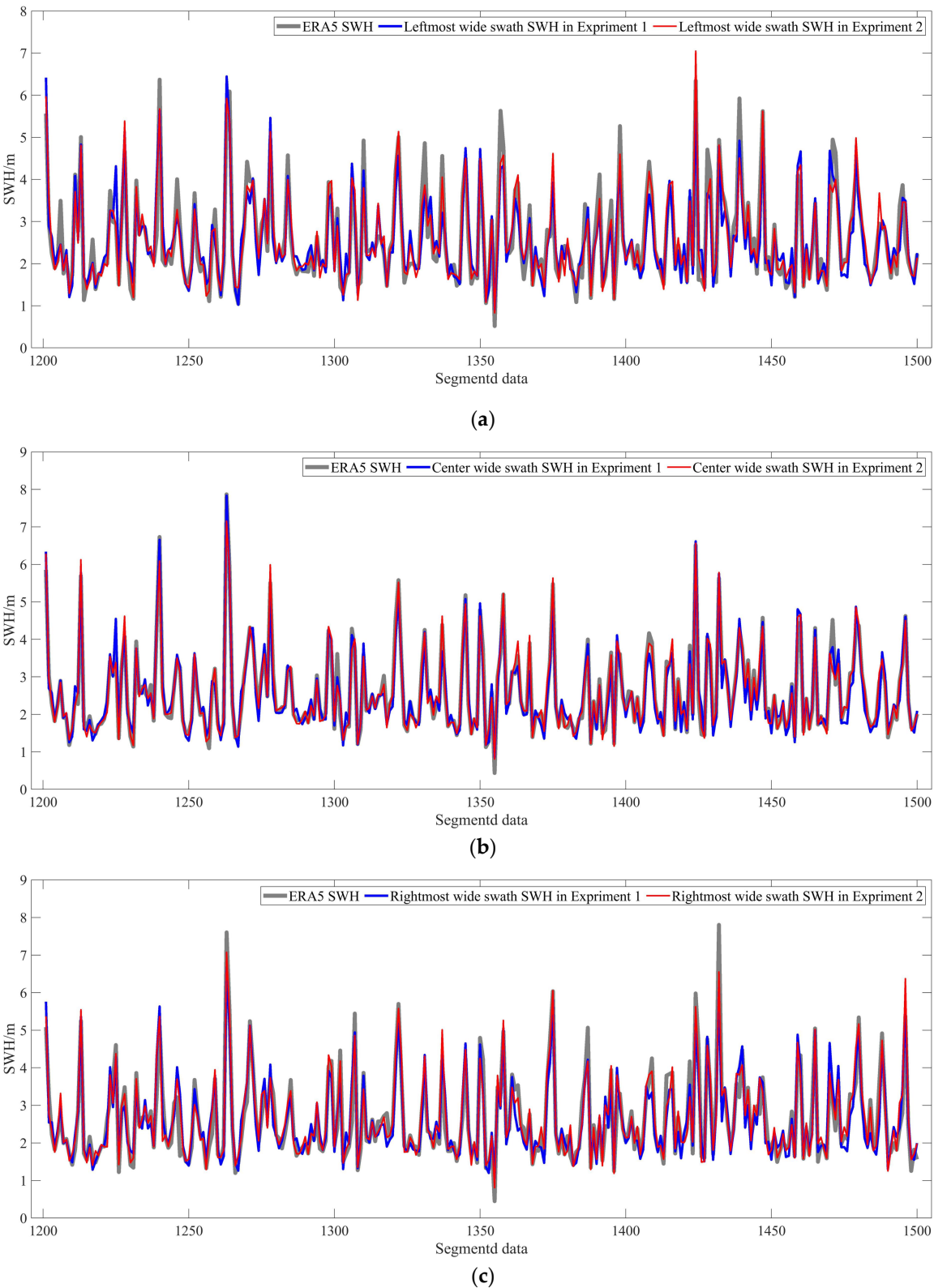
Figure 4. The line graphs of the segmented data. The leftmost, center and rightmost validation results of Experiments 1 (blue lines) and 2 (red lines) are denoted in (**a**)-(**c**), respectively.

(**a**)

(**b**)

(**c**) (**d**) (**e**)

(**f**) (**g**) (**h**)
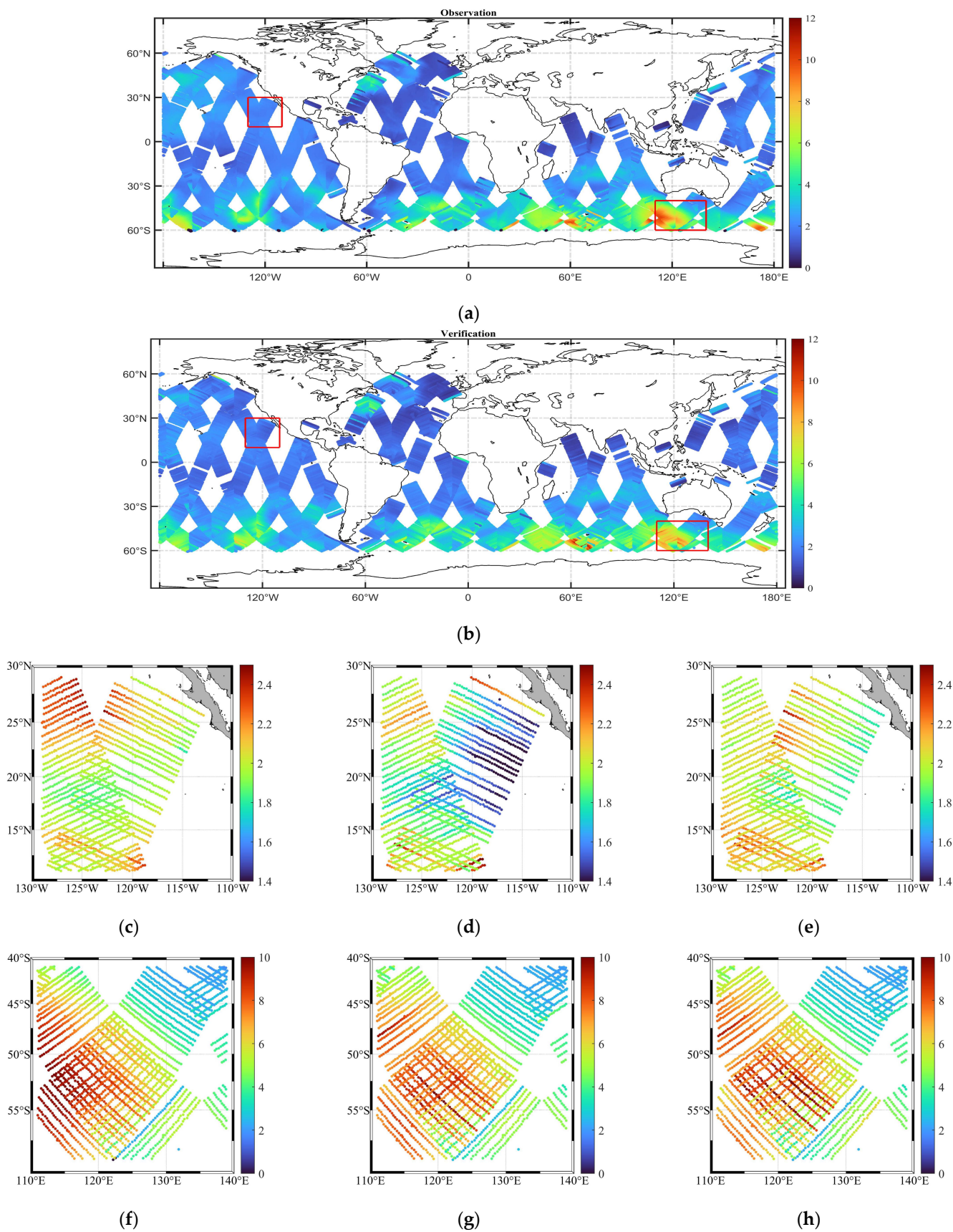
Figure 5. The results of the wide swath SWH. The observation (**a**) and the verification (**b**) of global wide swath SWH in Experiment 1, and the observation ((**c**), (**f**)) and the verification ((**d**) and (**g**) in Experiment 1, as well as (**e**) and (**h**) in Experiment 2) of their magnitude plots in northwestern area and southeastern area (the red boxes in (**a**) and **b**)), respectively.

From Figure 5a, it can be found that the data are distributed with a high probability between 1 and 5 m, and the values are generally larger than 5 m around 60° S. Numerical change in Figure 5b is basically consistent with the observations in Figure 5a. Two regions located in the northwest (130-110° W, 10-30° N) and southeast (110-140° E, 60-40° S) are drawn to manifest the detailed value intervals of wide swath SWH, respectively. Figure 5d and e fluctuate in a small range and the former has a difference of approximately 0.3 m compared to Figure 5c. Besides, the latter demonstrates a high consistency with Figure 5c. Combining with Figure 5f, Figure 5g exhibits a better performance than Figure 5h at larger values, which coincides with the phenomena reflected in Figure 4b. Figure 5g declares the expansion of the nadir SWH to generate a real-time grid product with wide swath along track, which can be employed as input for wave assimilation, spatial-temporal forecasting, extreme analysis and so on. Of course, it is undeniable that additionally considering swell into the input characteristics has a promising result when real-time is not strictly required. Furthermore, compared with Figure 1, our results extend the width of SWH to half of the wind field dimension, which demonstrates the effectiveness and feasibility of the model.

4. Conclusions

This paper employs the HY-2C data with simultaneously acquired wind and wave to build a deep learning model, the gate recurrent unit (GRU), obtaining a wide swath significant wave height (SWH) field along track. The Ku-band nadir SWH, as well as its latitude and longitude from altimeter are extracted to select the wind columns whose width occupy half of the scatterometer wind field dimension. The SWH of ERA5 is configured based on a time difference of half an hour and a spatial difference within 100 km. The validation data are segmented at a length of 300 and the center column outperformed the leftmost and rightmost columns under arbitrary interval, where the leftmost and rightmost columns are generally underestimated and slightly overestimated at the peaks and the troughs of wide swath SWH, respectively. The validation set with the length of 1-day at 10-second intervals is fed into the trained model, and the results show that a better fit appears, considering the swell to the input in the amplified northwestern area from 1.4 to 2.5 m. While in the southeast, its SWH ranges from 0 to 10 m and the model performs well without the swell feature for SWH larger than 7 m. When the data acquired by HY-2C are adopted as features and the data from ERA5 are utilized as the labels, a more time-sensitive grid product along track is generated. Nevertheless, when the data collected by HY-2C and the swell from ERA5 are applied as features, superior validation results are produced. Besides, the width of the SWH is extended to half of the wind field dimension, which could be further expanded or updated employing deep learning methods according to demands of the practical situation. The correlative wave parameters may be added appropriately to provide certain relevant information for the training model, so as to generate better grid products.

References

1. Guenaydin, K. The estimation of monthly mean significant wave heights by using artificial neural network and regression methods. *Ocean Engineering* **2008**, *35*(14-15), 1406-1415.
2. Lin, Y.P.; Huang, C.J.; Chen, S.H. Variations in directional wave parameters obtained from data measured using a GNSS buoy. *Ocean Engineering* **2020**, *209*, 107513.
3. Kang, J.; Mao, R.; Chang Y.; Fu, H. Comparative analysis of significant wave height between a new Southern Ocean buoy and satellite altimeter. *Atmospheric and Oceanic Science Letters* **2021**, *14*(C3), 100044.
4. Dobson, E.; Monaldo, F.; Goldhirsh J. Validation of Geosat altimeter-derived wind speeds and significant wave heights using buoy data. *Journal of Geophysical Research Oceans* **1987**, *92*(C10), 10719-10731.
5. Durrant, T.H.; Greenslade, D.J.M.; Simmonds, I. Validation of Jason-1 and Envisat Remotely Sensed Wave Heights. *Journal of Atmospheric and Oceanic Technology* **2009**, *26*(1), 123-134.
6. Bhowmick, S.A.; Sharma, R.; Babu, K.N.; Shukla A.K.; Kumar R.; Venkatesan R.; Gairola R.M.; Bonnefond P.; Picot N. Validation of SWH and SSHA from SARAL/AltiKa Using Jason-2 and In-Situ Observations. *Marine geodesy* **2015**, *38*, 193-205.
7. Kumar, U.M.; Swain, D.; Sasamal, S.K.; Reddy, N.N.; Ramanjappa, T. Validation of SARAL/AltiKa significant wave height and wind speed observations over the North Indian Ocean. *Journal of Atmospheric and Solar-Terrestrial Physics* **2015**, *135*, 174-180.
8. Sepulveda, H.H.; Queffeulou, P.; Ardhuin, F. Assessment of SARAL/AltiKa Wave Height Measurements Relative to Buoy, Jason-2, and Cryosat-2 Data. *Marine Geodesy* **2015**, *38*(sup1), 449-465.
9. Yang, J.; Zhang, J. Validation of Sentinel-3A/3B Satellite Altimetry Wave Heights with Buoy and Jason-3 Data. *Sensors* **2019**, *19*(13), 2914.
10. Yang, J.; Zhang, J.; Jia, Y.; Fan, C.; Cui, W. Validation of Sentinel-3A/3B and Jason-3 Altimeter Wind Speeds and Significant Wave Heights Using Buoy and ASCAT Data. *Remote Sensing* **2020**, *12*(13), 2079.
11. Chen, C.; Zhu, J.; Lin, M.; Zhao, Y.; Huang, X.; Wang, H.; Zhang Y.; Peng H. The validation of the significant wave height product of HY-2 altimeter–primary results. *Acta Oceanologica Sinica* **2013**, *32*(011), 82-86.
12. Wang, J.; Zhang, J.; Yang, J. The validation of HY-2 altimeter measurements of a significant wave height based on buoy data. *Acta Oceanologica Sinica* **2013**, *32*(011), 87-90.
13. Zhang H.; Qing W.U.; Chen G. Validation of HY-2A Remotely Sensed Wave Heights against Buoy Data and Jason-2 Altimeter Measurements. *Journal of Atmospheric & Oceanic Technology* **2015**, *32*(6), 150402094232008.
14. Wang, J.; Aouf, L.; Jia, Y.; Zhang Y. Validation and Calibration of Significant Wave Height and Wind Speed Retrievals from HY2B Altimeter Based on Deep Learning. *Remote Sensing* **2020**, *12*, 2858.
15. Liang, G.; Yang, J.; Wang J. Accuracy Evaluation of CFOSAT SWIM L2 Products Based on NDBC Buoy and Jason-3 Altimeter Data. *Remote Sensing* **2021**, *13*(5), 887.
16. Li, X.; Xu, Y.; Liu, B.; Lin, W.; He, Y.; Liu, J. Validation and calibration of Nadir SWH Products from CFOSAT and HY-2B with satellites and in situ observations. *Journal of Geophysical Research: Oceans* **2021**, *126*, e2020JC016689.
17. Zhang, L.; Zhang, L.; Du, B. Deep Learning for Remote Sensing Data: A Technical Tutorial on the State of the Art. *IEEE Geoscience and Remote Sensing Magazine* **2016**, *4*, 22-40.
18. Bentes, C.; Velotto, D.; Lehner, S. Target classification in oceanographic SAR images with deep neural networks: Architecture and initial results. *IEEE International Geoscience and Remote Sensing Symposium* **2015**, 3703-3706.
19. Shen, D.; Liu, B.; Li, X. Sea Surface Wind Retrieval from Synthetic Aperture Radar Data by Deep Convolutional Neural Networks. *IEEE International Geoscience and Remote Sensing Symposium* **2019**, 8035-8038.
20. Qin, T.; Jia, T.; Feng, Q.; Li, X. Sea surface wind speed retrieval from Sentinel-1 HH polarization data using conventional and neural network methods. *Acta Oceanologica Sinica* **2021**, *40*(1), 13-21.
21. Wang, J.K.; Aouf, L.; Dalphinet, A.; Li, B.X.; Xu, Y.; Liu, J.Q. Acquisition of the significant wave height from CFOSAT SWIM spectra through a deep neural network and its impact on wave model assimilation. *Journal of Geophysical Research: Oceans* **2021**, *126*, e2020JC016885.
22. Li X.; Yang D.; Yang J.; Zheng G.; Han G.; Nan Y.; Li W. Analysis of coastal wind speed retrieval from CYGNSS mission using artificial neural network. *Remote Sensing of Environment* **2021**, *260*, 112454.
23. Wang, J.K.; Aouf, L.; Badulin, S. Retrieval of wave period from altimetry: Deep learning accounting for random wave field dynamics. *Remote Sensing of Environment* **2021**, *265*, 112629.

328 24. Wang, J.K.; Aouf, L.; Dalphinet, A.; Zhang, Y.G.; Xu, Y.; Hauser, D.; Liu, J.Q. The Wide Swath Significant Wave Height: An
329   Innovative Reconstruction of Significant Wave Heights from CFOSAT's SWIM and Scatterometer Using Deep Learning.
330   *Geophysical Research Letters* **2021**, *48*, e2020GL091276.
331 25. Pang, D.; Tao, W. HY-2B and HY-2C Operational Satellites Under Development. *Aerospace China* **2016**, *17*(01), 69-69.
332 26. Ren Y. LM-4B Successfully Launched HY-2C Satellite. *Aerospace China* **2020**, *21*(03), 56.
333 27. Jia, Y.; Lin M.; Zhang Y. Evaluations of the Significant Wave Height Products of HY-2B Satellite Radar Altimeters. *Marine*
334   *Geodesy* **2020**, *43*(4), 396-413.
335 28. Wang, Z.; Zou, J.; Stoffelen, A.; Lin, W.; Verhoef, A.; Li X.; He Y.; Zhang Y.; Lin M. Scatterometer Sea Surface Wind Product
336   Validation for HY-2C. *IEEE Journal of Selected Topics in Applied Earth Observations and Remote Sensing* **2021**, *14*, 6156-6164.
337 29. Hersbach, H.; Bell, B.; Berrisford, P., et al. The ERA5 global reanalysis. *Quarterly Journal of the Royal Meteorological Society* **2020**,
338   *146*(730), 1999–2049.